



ELSEVIER

Contents lists available at ScienceDirect

Journal of Luminescence

journal homepage: [www.elsevier.com/locate/jlumin](http://www.elsevier.com/locate/jlumin)

# Synthesis and optical properties of Er<sup>3+</sup> and Eu<sup>3+</sup> doped SrAl<sub>2</sub>O<sub>4</sub> phosphor ceramic

M. Ayvaci<sup>a</sup>, A. Ege<sup>a</sup>, S. Yerci<sup>b</sup>, N. Can<sup>a,\*</sup>

<sup>a</sup> Celal Bayar University, Faculty of Arts and Sciences, Department of Physics, 45010 Muradiye-Manisa, Turkey

<sup>b</sup> Department of Electrical and Computer Engineering, Boston University, 8 Saint Mary's street, Boston, MA 02215-2421, USA

## ARTICLE INFO

### Article history:

Received 4 February 2011

Received in revised form

25 April 2011

Accepted 30 May 2011

Available online 30 June 2011

### Keywords:

Strontium aluminate

Rare earths

Optical properties

Photoluminescence

Raman scattering

SEM

## ABSTRACT

We report, for the first time on luminescence from a Er<sup>3+</sup> doped SrAl<sub>2</sub>O<sub>4</sub> phosphor. Effects of Eu<sup>3+</sup> doping were also studied. The influence of rare-earth doping in crystal structure and its optical properties were analysed by means of X-ray diffraction (XRD), Raman scattering, optical absorption, excitation and emission (PL) spectroscopy, thermally stimulated luminescence (TSL) and scanning electron microscope (SEM). Luminescence spectra and luminescence decay curves for Er<sup>3+</sup> transitions in the near infrared region were recorded. The PL maximum for Eu doped SrAl<sub>2</sub>O<sub>4</sub> is obtained at 620 nm and corresponds to the orange region of the spectrum. Diffraction patterns reveal a dominant phase, characteristic of the monoclinic SrAl<sub>2</sub>O<sub>4</sub> compound and the presence of dopants has no effect on the basic crystal structure of SrAl<sub>2</sub>O<sub>4</sub>. The shapes of the glow curves are different for each dopant irradiated with either a <sup>90</sup>Sr–<sup>90</sup>Y beta source, or UV light at 311 nm, and in detail the TL signals differ somewhat between Er and Eu dopants.

© 2011 Elsevier B.V. All rights reserved.

## 1. Introduction

Materials that present long lasting phosphorescence (LLP) are potential candidates for use in photonics applications, such as display technology and lighting. Among others, strontium based aluminate phosphors are well known for their high quantum efficiency, long-lived afterglow, good chemical stability and other excellent luminescent features, which make them appropriate candidates to replace the traditional II–VI based phosphors. These materials are successfully used in various applications from luminous paints for highways, airport, buildings, ceramic products, textile industry, the dial plate of glow watches, to warning signs and escape routes, etc. [1,2]. In recent years, the strontium aluminates have attracted intense research, since they have excellent properties such as high quantum efficiency, long persistence of phosphorescence and good stability. Also, the importance of rare earth ions as efficient emitter in a variety of solid-state matrices is well known. Among rare earth ions, Europium (Eu) is often employed by researchers for making red emitting phosphors where the prominent 612 nm emission band arises from electric dipole moment allowed transitions [3]. These properties have been observed in the following compounds: SrAl<sub>2</sub>O<sub>4</sub>:Eu<sup>2+</sup>, Dy<sup>3+</sup>, B<sup>3+</sup> [4], Sr<sub>4</sub>Al<sub>14</sub>O<sub>25</sub>:Eu<sup>2+</sup>, Dy<sup>3+</sup>, B<sup>3+</sup> [5], SrAl<sub>4</sub>O<sub>7</sub>:Eu<sup>2+</sup>, Dy<sup>3+</sup> [6], SrAl<sub>12</sub>O<sub>19</sub>:Eu<sup>2+</sup>, Dy<sup>3+</sup>, Sr<sub>2</sub>Al<sub>6</sub>O<sub>11</sub>:Eu<sup>2+</sup>, Dy<sup>3+</sup> [7], SrAl<sub>2</sub>O<sub>4</sub>:Eu<sup>2+</sup>,

Dy<sup>3+</sup> [8]. In addition to a higher chemical stability, the intensity and the duration of the phosphorescence of strontium aluminates (in especially SrAl<sub>2</sub>O<sub>4</sub>:Eu<sup>2+</sup>, Dy<sup>3+</sup>, B<sup>3+</sup>) makes it possible to envisage a continuous light emission during a whole night (10 h), hence greatly renewing interests in the phosphorescence phenomenon. Potential applications of these compounds are numerous, especially in the areas of safety sign improvements and energy saving (e.g., traffic signs, emergency signs, safety clothes, advertising, etc.). The other rare-earth ions have been of interest to study the effect on optical properties of this phosphor host. There is a comparative lack of information related to optical properties of the present phosphor in the scientific literature. Additionally, to the best of our knowledge, the effect of Er doping in SrAl<sub>2</sub>O<sub>4</sub> host has not been reported so far. A need for information on the results of Er doping has thus motivated the present work.

## 2. Material and methods

All samples used in this work were prepared from stoichiometric amounts of high purity (Sigma-Aldrich > 99.99%) SrO, Al<sub>2</sub>O<sub>3</sub> and H<sub>3</sub>BO<sub>3</sub> as a flux and rare earth oxides with compositions of 2SrO–Al<sub>2</sub>O<sub>3</sub>–H<sub>3</sub>BO<sub>3</sub>–1%RE (Eu<sub>2</sub>O<sub>3</sub>, and Er<sub>2</sub>O<sub>3</sub>). A batch was created from the samples obtained by mixing in an agate mortar under a nitrogen atmosphere. The contribution of all rare earth elements in the batch is 1 mol%. Raw materials are placed in a high temperature furnace using a platinum crucible.

\* Corresponding author. Tel.: +90 236 241 21 56; fax: +90 236 241 21 58.  
E-mail address: [cannurdogan@yahoo.com](mailto:cannurdogan@yahoo.com) (N. Can).

Samples, under a reduced atmosphere (15% H<sub>2</sub> and 85% N<sub>2</sub>), were sintered at 1650 °C for 2 h, and then are allowed to cool for about 24 h in the furnace. Note that this slow cooling provides the formation of ceramic structure for these materials, but more rapid cooling results in a more glassy form of the material. XRD measurements were carried out using a Philips X'Pert Pro X-ray diffractometer with Bragg Brentano geometry using CuK $\alpha$  line ( $\lambda=1.5418$  Å) for the identification of crystallographic phases. The morphology and particle size of the prepared powders were observed with scanning electron microscopy (Jeol/JSM-6335 F/INCA-EDS, SEM). Irradiation of the samples was performed with a <sup>90</sup>Sr–<sup>90</sup>Y beta source (650 MBq) and UV source at 311 nm (Philips TL 100 W/01 SLV) and experiments were performed immediately after irradiation in order to minimize any fading effect. The thermally stimulated luminescence (TSL) glow curves were recorded with a TLD reader (Harshaw Model 3500). A heat absorbent filter (Schott KG-1) has been placed in front of the PM tube in order to prevent the blackbody radiation reaching the PM tube. The glow curves of undoped SrAl<sub>2</sub>O<sub>4</sub>, SrAl<sub>2</sub>O<sub>4</sub>:Eu and SrAl<sub>2</sub>O<sub>4</sub>:Er samples were obtained in the temperature range 50–600 °C with linear heating rate of 2 °C s<sup>-1</sup> after beta or UV (311 nm) irradiation.

For the measurements of Er photoluminescence (PL) spectrum and PL lifetime, the sample was excited resonantly using a 488 nm line of an Ar ion laser (Spectra Physics, 177–602) modulated by a mechanical chopper and detected using an extended photomultiplier tube (Hamamatsu R5509–73) detector. The detector was coupled to an oscilloscope for the lifetime measurements. The PL measurements of Eu doped SrAl<sub>2</sub>O<sub>4</sub> samples were performed on a computer-controlled fluorescence spectrometer with excitation at 234 nm.

Dispersive confocal micro-Raman study on the samples was performed in the condition of dark background at room temperature using a HORIBA Jobin Yvon Scientific XPLORE dispersive confocal micro-Raman spectrometer (DCMRS) with high throughput integrated spectrograph. The samples are irradiated with a monochromatic light source (532 nm laser) through a microscope. The Si Raman line at 520 cm<sup>-1</sup> was used for a frequency

calibration of the Raman lines. The spectral line width was smaller than 3 cm<sup>-1</sup>.

### 3. Results and discussion

#### 3.1. X-ray diffraction analysis

The analysis of XRD data of SrAl<sub>2</sub>O<sub>4</sub> phases is usually qualitative, just based on relative peak intensities. XRD was used to identify the presence of any impurity phases of compositions different from SrAl<sub>2</sub>O<sub>4</sub>. A typical X-ray diffraction pattern of the resultant SrAl<sub>2</sub>O<sub>4</sub>:Er<sup>3+</sup>, Eu<sup>3+</sup> are shown in Fig. 1. The XRD pattern for the parent SrAl<sub>2</sub>O<sub>4</sub> is also given for comparison. The monoclinic phase diffraction peaks of the parent SrAl<sub>2</sub>O<sub>4</sub> are clearly observed in the XRD patterns. The XRD patterns were similar for all the prepared samples and hence are not reported to avoid repetition. No peak other than those from the parent are resolved in the XRD pattern, which suggests the formation of single phase material. The lattice parameters were calculated from the XRD data on the basis of the parent SrAl<sub>2</sub>O<sub>4</sub>. The lattice parameters calculated were for monoclinic SrAl<sub>2</sub>O<sub>4</sub>,  $a \approx 8.440$  Å,  $b \approx 8.821$  Å,  $c \approx 5.157$  Å,  $\beta \approx 93.4^\circ$ , with no measurable change in the cell volume. It is to be noted that the small amount of doped rare-earth active ions Er<sup>2+</sup>, Sm<sup>2+</sup>, Dy<sup>2+</sup> and Eu<sup>2+</sup> have almost no effect on the basic crystal structure of SrAl<sub>2</sub>O<sub>4</sub>. Note XRD data doped with the other rare earth ions are not shown here. Also in the figure we have identified the principal peaks of the ( $\bar{2}11$ ), (2 2 0), (2 1 1) and (0 3 1) planes that characterize the crystalline SrAl<sub>2</sub>O<sub>4</sub> structure; according to registers in the International Centre for Diffraction Data (ICDD) database (JCPDS 74-0794). The crystal structure of SrAl<sub>2</sub>O<sub>4</sub> is derivative of the stuffed tridymite (SiO<sub>2</sub>) structure, in which all of the Si<sup>4+</sup> is replaced by Al<sup>3+</sup> and the charge compensating cation Sr<sup>2+</sup> occupy the large open channels in the framework. This structure is less regular compared to the hexagonal structure of SrAl<sub>2</sub>O<sub>4</sub> [9,10]. The schematic views of the monoclinic SrAl<sub>2</sub>O<sub>4</sub> are shown in Fig. 2. There are two crystallographically different sites for Sr<sup>2+</sup>, which have identical coordination numbers (i.e. 6+1). The two environments differ only by a slight distortion of

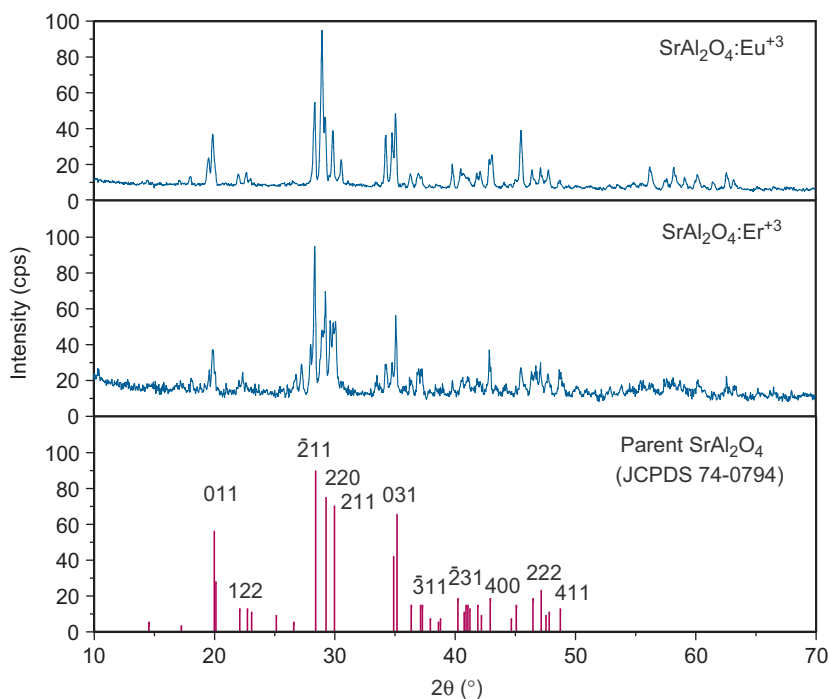


Fig. 1. X-ray diffraction pattern of Er<sup>3+</sup> and Eu<sup>3+</sup> doped SrAl<sub>2</sub>O<sub>4</sub> and principal peaks of crystalline planes that characterized SrAl<sub>2</sub>O<sub>4</sub> host structure.

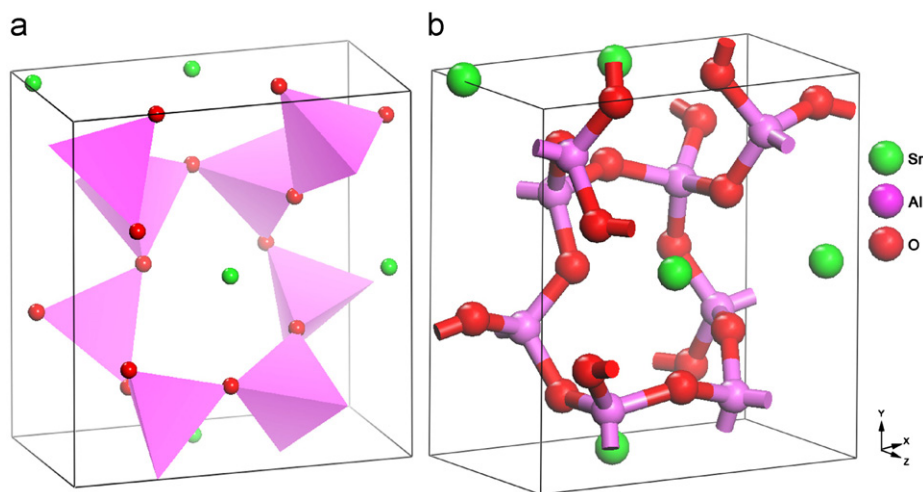


Fig. 2. The schematic view of the monoclinic  $\text{SrAl}_2\text{O}_4$ : (a) polyhedron and (b) ball and stick representation.

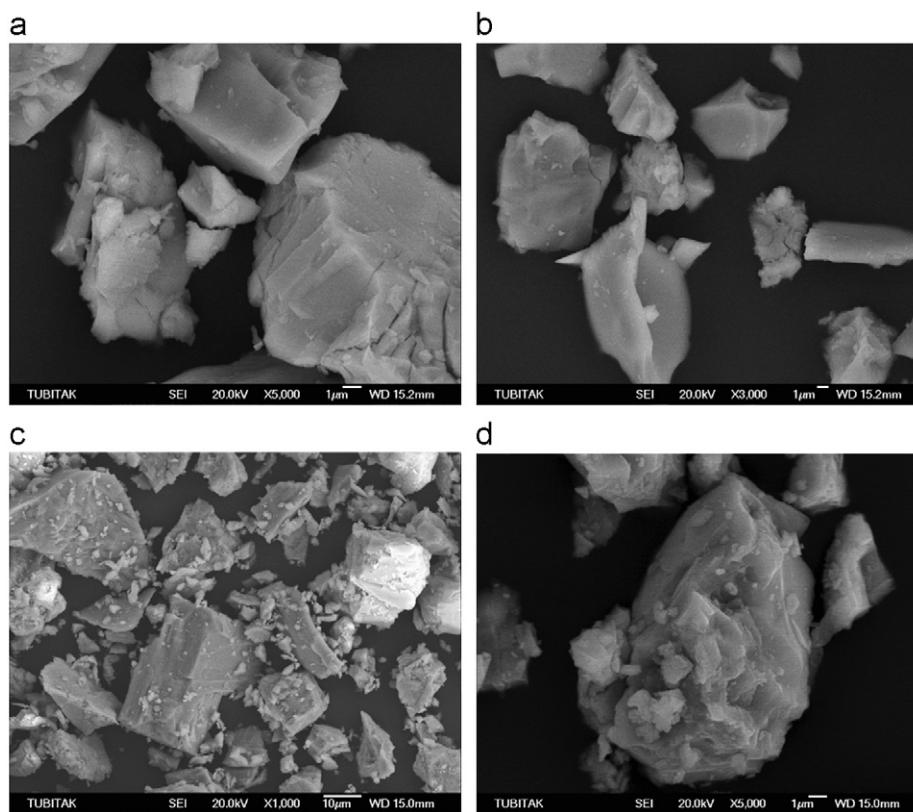


Fig. 3. Representative SEM micrographs for  $\text{SrAl}_2\text{O}_4:\text{Eu}^{3+}$  (top),  $\text{Er}^{3+}$  (bottom).

their square planes. The  $\text{Sr}^{2+}$  and  $\text{Eu}^{2+}$  ions are very similar in their ionic radii (i.e., 1.21 and 1.20 Å, respectively). Consequently, when occupied by  $\text{Eu}^{2+}$  ions, the two different  $\text{Sr}^{2+}$  sites will have a quite similar local distortion, so that the  $\text{Eu}^{2+}$  ions located at the two different  $\text{Sr}^{2+}$  sites will have very similar local environments.

An Er ion preferentially enters into the substitutional Si sites due to similar ionic radius of Si rather than Al sites. However, the Si replaced by Er may form Si-rich phase. Since the percentage of doping is small, it is not reflected in XRD. Therefore the second dopant  $\text{Er}^{3+}$  ion also occupies the  $\text{Sr}^{2+}$  site.

In conclusion no other product or starting material was observed, implying that the phase composition of the samples is all low-temperature monoclinic phase ( $\alpha$ -phase), and a small

amount of doped  $\text{Er}^{3+}$  and  $\text{Eu}^{3+}$  ions have no obvious influence on the structure of the host due to the similar ionic radius.

### 3.2. SEM analysis

An SEM study was carried out to investigate the surface morphology and the crystallite size of the synthesized phosphors. Fig. 3(a–d) shows the representative SEM micrographs taken for  $\text{SrAl}_2\text{O}_4:\text{Eu}^{3+}$ ,  $\text{SrAl}_2\text{O}_4:\text{Er}^{3+}$  (1% mol Eu and %1 mol Er) at different magnifications, respectively. The micrographs show that the crystallite sizes are varying from few microns to several tens of microns. The crystallites have sharp surface morphology of single crystalline grains. It was observed that the crystallite sizes are nearly same irrespective of

the composition. The results show that the doping process does not make significant changes to the morphology and size of the nanostructures. Compared with phosphors prepared via other techniques, the grain sizes seen here are larger. In the other techniques (i.e. combustion method) the phosphor powders are irregular spherical particles, the surfaces of the foams show a lot of cracks, voids and pores formed by the escaping gases during combustion reaction. In fact, the large amount of escaping gases dissipates heat and thereby prevents the material from sintering and thus provides conditions for formation of nanocrystalline phase. It is ascribed to that the solid state reaction used in this study requires a high calcinating temperature, which induces sintering and aggregation of particles, and it is an advantage for perfect crystal formation.

### 3.3. Raman scattering

Raman spectroscopy is very sensitive to the structure and bond order of metal oxides, especially in the region of metal–oxygen stretching modes, because many of the Raman frequencies depend on the bond order in the structure. A higher metal–oxygen bond order, corresponding to a shorter bond distance, shifts the Raman band to higher wave numbers. In order to complement XRD data, Raman spectroscopy has been used for determining the coexistence of monoclinic and hexagonal polymorphs in earlier reports [11]. Unfortunately there is a very limited literature on this topic. A precise assignment of peaks appearing in this spectrum is almost impossible, due to the large numbers of modes expected for this phase (81), but the sensibility of this technique allows one to know if a percentage of this phase is present in the sample. Therefore, we can only give general comments about the origin of the modes, and will use this technique mainly for phase identification (see Figs. 4 and 5). The spectrum exhibits a ubiquitous  $465\text{ cm}^{-1}$  band attributed to the bending of O–Al–O bonds in corner-sharing tetrahedra, indicating that the polymorphs present very closely structures (Fig. 4). As regards the interpretation of the Raman spectrum, the lack of polarization measurements and the expected mixing of atomic shifts prevent mode assignment. In the case of framework structures built up of linked tetrahedral units, it is usual to discuss the Raman spectrum in terms of internal vibrations of the  $\text{MO}_4$  unit. To a first approximation, we attribute modes at frequency higher than  $600\text{ cm}^{-1}$  to Al–O bond-stretching vibrations and the narrow, low-frequency peaks below  $150\text{ cm}^{-1}$  to tetrahedral librations or tilts. In the intermediate region the assignment is

challenging but, by analogy with other compounds, we assign the most intense band at  $465\text{ cm}^{-1}$  to the bending vibration of the O–Al–O angle aforementioned before. A remarkable fact is that the  $465\text{ cm}^{-1}$  mode is the only one that remains with high intensity in highly disordered or non-crystallized compositions, such as those annealed at low temperatures, which suggests that the  $[\text{AlO}_4]$  unit is stabilized first as a rigid unit, and that disorder arises solely from the orientation of such units and/or slight oxygen displacements. Higher Raman shifts are probably due to multiphonon or electronic Raman processes.

### 3.4. Optical absorption measurements

#### 3.4.1. Eu doped $\text{SrAl}_2\text{O}_4$

Fig. 6 shows the absorption spectrum of Eu doped  $\text{SrAl}_2\text{O}_4$  samples in the spectral region from 200 to 800 nm at room temperature. The absorption profiles exhibit broad bands in the UV region (below 350 nm). One band in the short UV region (peak at 275 nm) should originate from the charge transfer band (CTB) of  $\text{Eu}^{2+}-\text{O}^{2-}$  bond [12]. The energy position of this band is closely related to the covalence of  $\text{Eu}^{2+}-\text{O}^{2-}$  bond and the coordination number of  $\text{Eu}^{2+}$ . The fundamental absorption band in  $\text{SrAl}_2\text{O}_4$  structure has been observed at about 200 nm [13,14]. In our case we found that this band is located at 217 nm. Thus, the band at 265 nm may be related to both the  $\text{Eu}^{2+}-\text{O}^{2-}$  and the absorption matrix.

#### 3.4.2. Er doped $\text{SrAl}_2\text{O}_4$

Fig. 7 shows absorption spectrum of Er doped  $\text{SrAl}_2\text{O}_4$  in the range of 200–800 nm at room temperature. In accordance with the energy level diagram and the literature data [15], all the observed absorption bands (Fig. 7) were assigned to appropriate f–f electronic transitions of  $\text{Er}^{3+}$  ions from the  $^4\text{I}_{15/2}$  ground state to the following excited states:  $^4\text{G}_{11/2}$ ,  $^2\text{H}_{9/2}$ ,  $^4\text{F}_{3/2}$ ,  $^4\text{F}_{5/2}$ ,  $^4\text{F}_{7/2}$ ,  $^2\text{H}_{11/2}$ ,  $^4\text{S}_{3/2}$ ,  $^4\text{F}_{9/2}$ ,  $4\text{I}_{9/2}$  and  $^4\text{I}_{9/2}$ . No bands characteristic for  $\text{Er}^{2+}$  ions were observed in the optical absorption spectrum of  $\text{SrAl}_2\text{O}_4:\text{Er}$  glass, confirming that incorporation of the erbium impurity into the  $\text{SrAl}_2\text{O}_4$  is in the  $\text{Er}^{3+}$  valence state. However, in the shorter wavelength region of 200–400 nm, the bands are overlapped with each other quite strongly and exhibit strong background absorption. As far as we are aware the optical absorption behaviour of Er ions in pure  $\text{SrAl}_2\text{O}_4$  phase has not been reported.

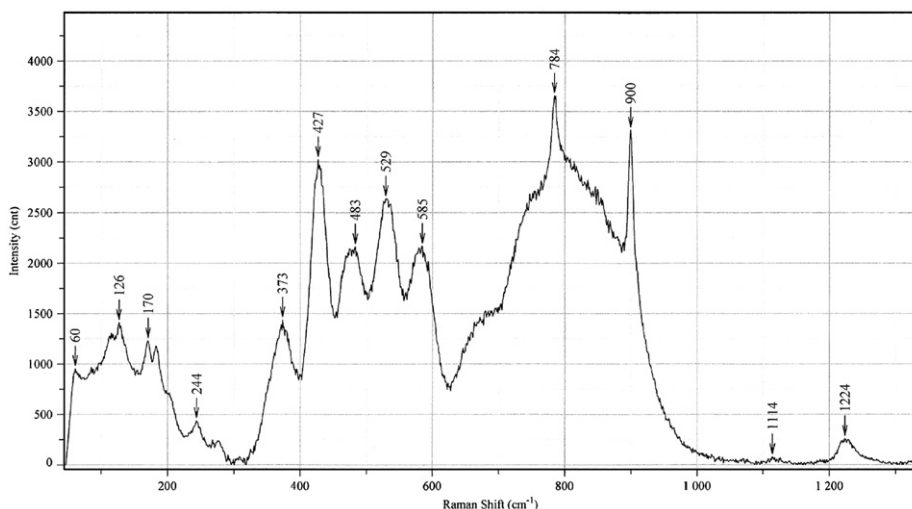


Fig. 4. Raman spectrum of Er doped  $\text{SrAl}_2\text{O}_4$ .

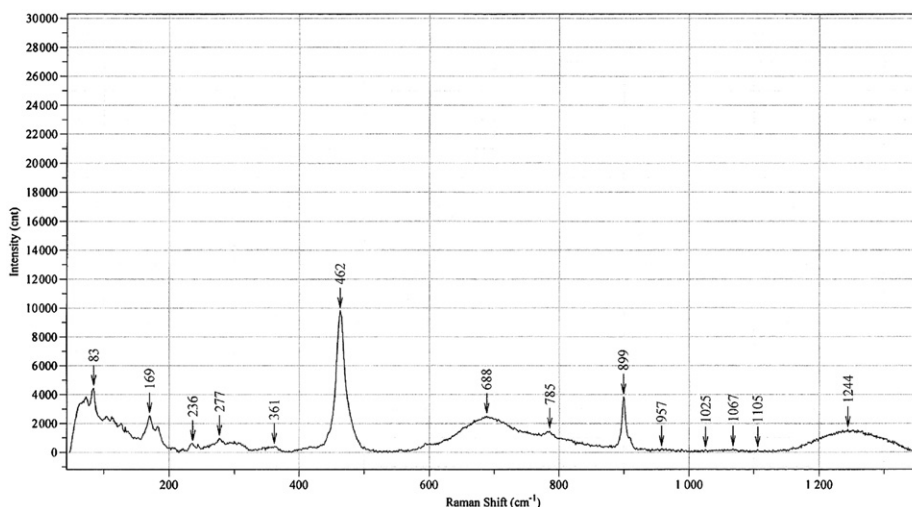


Fig. 5. Raman spectrum of Eu doped SrAl<sub>2</sub>O<sub>4</sub>.

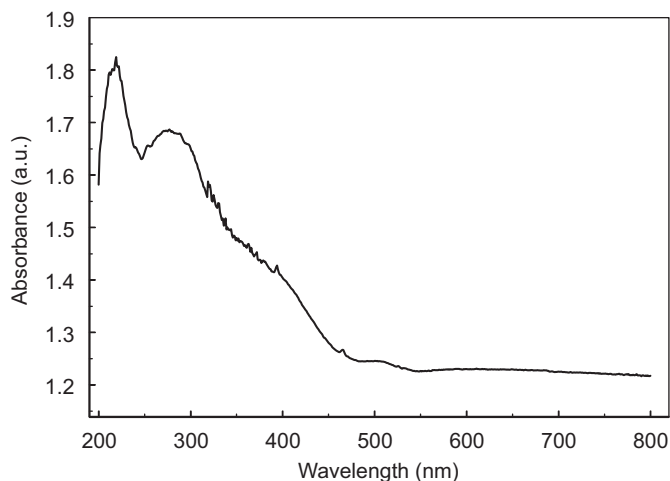


Fig. 6. UV/Vis absorption spectrum of Eu doped SrAl<sub>2</sub>O<sub>4</sub>.

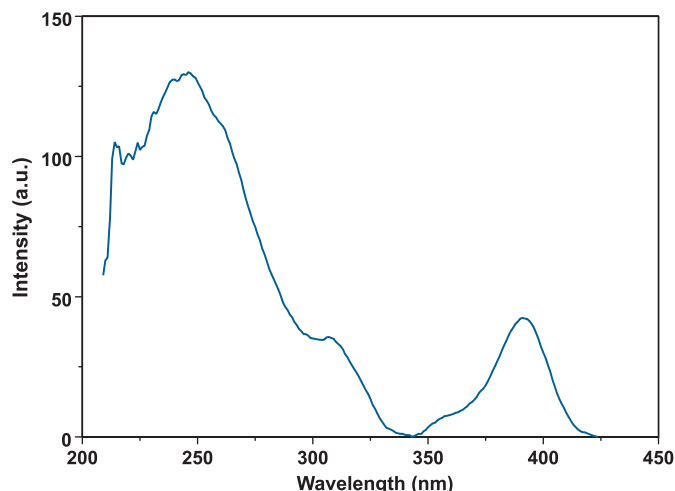


Fig. 8. PL excitation spectrum of Eu doped SrAl<sub>2</sub>O<sub>4</sub>.

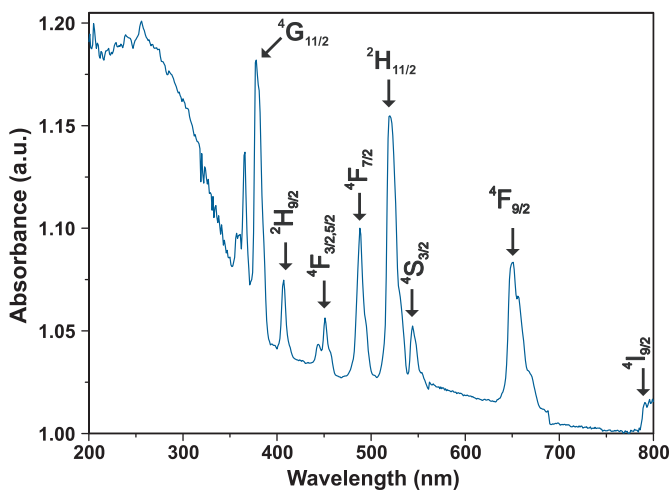


Fig. 7. UV/Vis absorption spectrum of Er doped SrAl<sub>2</sub>O<sub>4</sub>.

### 3.5. Photoluminescence

#### 3.5.1. Eu doped SrAl<sub>2</sub>O<sub>4</sub>

Previous works do not report a plausible number of experimental lines associated to Eu<sup>3+</sup> transitions. Page et al. [16]

showed the emission spectra for different concentration of Eu<sup>3+</sup>, but the transitions were not clearly identified. Sharma et al. [3], did not show the emission spectral region associated to the <sup>5</sup>D<sub>0</sub>→<sup>7</sup>F<sub>j</sub> (j=3, 4) emission lines of the Eu<sup>3+</sup> ions and Pan et al. [17] did not describe the <sup>5</sup>D<sub>0</sub>→<sup>7</sup>F<sub>4</sub> in the emission spectra for Eu<sup>3+</sup>. The excitation and emission spectra of phosphors SrAl<sub>2</sub>O<sub>4</sub> doped with Eu are shown in Figs. 8 and 9, respectively. The excitation spectrum consists of three bands centred at 250, and 310 and 370 nm, respectively (Fig. 8). The band at 250 nm is attributed to ligand to metal charge transfer (LMCT) state from fully filled 2p-orbitals of O<sup>2-</sup> to partially filled 4f<sup>7</sup> levels of Eu<sup>3+</sup> [17]. The peak centre at 370 nm is due to the 4f–5d transition of Eu<sup>2+</sup> ion. The results show that the compounds could be excited by ultraviolet and visible light. For the 5d electron lies in external layer in a naked and unshielded state, the splitting of energy level is strongly affected by the crystal field, and it makes the 4f<sup>6</sup>5d→4f<sup>7</sup> (<sup>8</sup>S<sub>7/2</sub>) transition of Eu<sup>2+</sup> ion broad. We observed that the intensities of emission increase with the increasing of the H<sub>3</sub>BO<sub>3</sub> concentration. H<sub>3</sub>BO<sub>3</sub> makes the crystalline growth temperature low and greatly promotes the reaction process, the concentration of Eu<sup>2+</sup> in crystal lattice increases. When adding more H<sub>3</sub>BO<sub>3</sub>, the presence of borate in vitreous state lowers the luminescence intensity. In the excitation spectra, a broad excitation band centred at 370 nm could be due to existence of intermediate

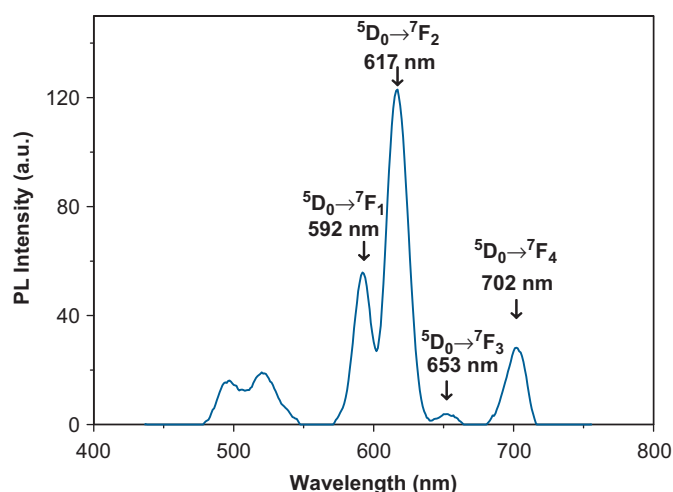


Fig. 9. PL emission spectrum of Eu doped SrAl<sub>2</sub>O<sub>4</sub> taken with excitation at 234 nm.

trapping states (ITS). It is seen that the intensity of charge transfer transition at 250 nm is stronger than the 370 nm transition. The phenomenon is common because the typical Eu<sup>3+</sup> activated phosphors show strong charge transfer transitions absorption band. Thus, it is anticipated that sufficient energy-transfer takes place between the host and the activator. Consequently, the emission spectrum of this sample was registered at 313 nm excitation wavelength.

The resulting emission spectrum is depicted in Fig. 9. The intense peak at about 520 nm is associated with Eu<sup>2+</sup> transitions [18] and indicates the presence of reduced europium in the sample. After excitation, the emission spectra are described by well-known <sup>5</sup>D<sub>0</sub>→<sup>7</sup>F<sub>*J*</sub> (*J*=0, 1, 2, 3,...) emission lines of the Eu<sup>3+</sup> ion, with strong emission at 620 nm (<sup>5</sup>D<sub>0</sub>→<sup>7</sup>F<sub>2</sub>). In our case, the intermediate state is thought to populate the lowest <sup>5</sup>D<sub>0</sub> state leading to the emission at 620 nm. Other emission bands were observed at 590, 650 and 700 nm. If there is no inversion at the site of the rare earth ion, the electric dipole transitions exists, and the maximum emission is obtained at 650 nm, which is sensitive to the ligand environment. But if 620 nm band is predominant, the magnetic dipole transition is predominant, which indicates that the Eu<sup>3+</sup> ions lie in central symmetric sites. The possibility of transition in any symmetry is based on the prevailing selection rules. For no centre of inversion symmetry, electron dipole transitions can occur and correspond to Δ*J*= ±2 as selection rules. But if, Eu<sup>3+</sup> ion is a centre of inversion symmetry for surrounding atoms in the lattice, only magnetic dipole transition are allowed and selection rules of Δ*J*= ±1 are operative. <sup>5</sup>D<sub>0</sub>→<sup>7</sup>F<sub>1</sub> transition is forbidden as electric dipoles but allowed as magnetic dipoles and all lines corresponding to these transitions split into number of components decided by the local symmetry. In our case, the latter option is more probable. The emission lines at 590, 650, 700 nm corresponds to <sup>5</sup>D<sub>0</sub>→<sup>7</sup>F<sub>1</sub>, <sup>5</sup>D<sub>0</sub>→<sup>7</sup>F<sub>4</sub> and <sup>5</sup>D<sub>0</sub>→<sup>7</sup>F<sub>4</sub> transitions, respectively. Note that several literature examples suggest emission from Eu doped SrAl<sub>2</sub>O<sub>4</sub> materials can occur in these regions [3,19].

### 3.5.2. Er doped SrAl<sub>2</sub>O<sub>4</sub>

In the present investigation we present a spectroscopic study of SrAl<sub>2</sub>O<sub>4</sub> powder sample doped with the Er<sup>3+</sup>, with the purpose of assessing its potentialities for technological applications. However, the choice of the Er host depends on the materials properties required by the specific optical function which has to be realized. In general, erbium luminescence at 1.54 μm arises from a sharp

atomic-like radiative transition between the <sup>4</sup>I<sub>13/2</sub> state and the <sup>4</sup>I<sub>15/2</sub> state (ground level). This transition is forbidden in the isolated Er<sup>3+</sup> due to the electric dipole selection rules, while it is allowed for Er<sup>3+</sup> in a host matrix due to the interaction with the crystalline field. The lifetime of this transition depends on the host material and is usually on the order of a few milliseconds. For optical applications it is necessary to incorporate Er<sup>3+</sup> within the host matrix and to excite it optically or electrically to the <sup>4</sup>I<sub>13/2</sub> level.

Fig. 10 reports a room temperature photoluminescence spectrum Er in SrAl<sub>2</sub>O<sub>4</sub> powder sample. The spectrum shows peaks at 1.530 and 1.544 μm characteristic for the intra-4f shell transitions between the <sup>4</sup>I<sub>13/2</sub> and <sup>4</sup>I<sub>15/2</sub> manifolds of Er<sup>3+</sup>. The pump laser excites Er<sup>3+</sup> from the ground state (<sup>4</sup>I<sub>15/2</sub>) to the <sup>2</sup>H<sub>11/2</sub> manifold and rapid non-radiative relaxation leads the system to the metastable <sup>4</sup>I<sub>13/2</sub> manifold from which the radiative transition then takes place. The luminescence decay curve shown in Fig. 11 provides information on the relaxation dynamics of the excited states. The curve was acquired at room temperature upon direct

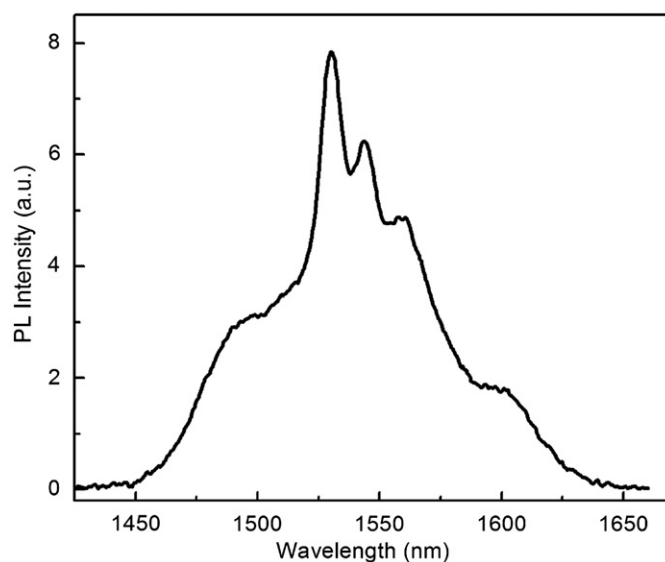


Fig. 10. Room temperature emission spectrum related to the <sup>4</sup>I<sub>13/2</sub>–<sup>4</sup>I<sub>15/2</sub> transition of Er<sup>3+</sup> in SrAl<sub>2</sub>O<sub>4</sub> excited at 488 nm.

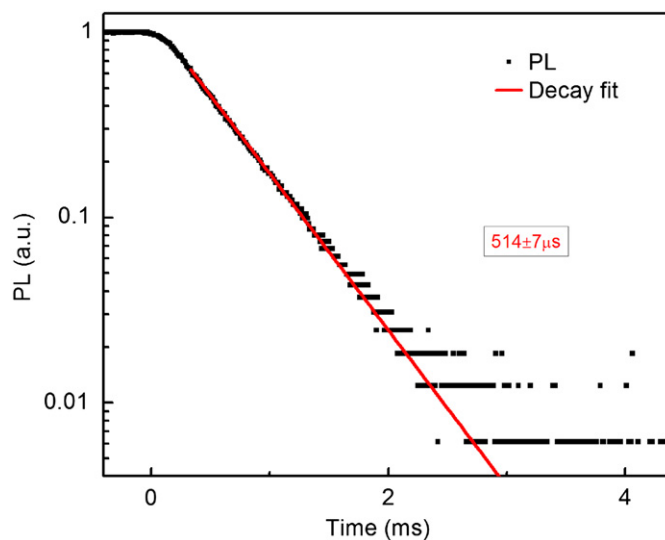


Fig. 11. Semilog plot of luminescence decay curve recorded at room temperature upon direct excitation of emitting levels.

excitation of the luminescent level. It appears as straight lines in semilog plots implying that the decay follows single exponential time dependence. Relaxation of excited states of rare earth ions in phosphor materials is governed by competing radiative decay, multiphonon relaxation and non-radiative ion–ion interaction. The lifetime of the powders is 514  $\mu\text{s}$ . In general, in  $\text{Er}^{3+}$ -doped materials the up-conversion process could be achieved by either through excited state absorption (ESA) and/or energy transfer pumping mechanisms but in our case there is no evidence of up-conversion due to the lack of 980 nm emission.

### 3.6. Thermally stimulated luminescence characteristics

The phosphors were subjected to the TSL study to ascertain the defects present in the synthesized compounds. TSL glow curve of undoped  $\text{SrAl}_2\text{O}_4$  sample shows four peaks at 82, 153, 270 and 397  $^\circ\text{C}$  after beta irradiation, although it has only a very low TSL intensity at about background level after UV irradiation in undoped material (Fig. 12). By contrast, Er and Eu doped  $\text{SrAl}_2\text{O}_4$  samples display very intense luminescence signal after UV irradiation. There are many overlapping peaks having maximum at 104, 157, 230 and 337  $^\circ\text{C}$  in the glow curve of Er doped  $\text{SrAl}_2\text{O}_4$  after UV illumination. On the other hand, the glow curve of the Eu doped sample has two peaks at 117 and 527  $^\circ\text{C}$  and its maximum luminescence intensity is about hundred times of that of Er doped sample for the same amount of UV illumination (Fig. 13).

Fig. 14 indicates the TSL glow curves of beta irradiated  $\text{SrAl}_2\text{O}_4:\text{Eu}$  and  $\text{SrAl}_2\text{O}_4:\text{Er}$  phosphor. There are four peaks at 93, 225, 345 and 471  $^\circ\text{C}$  in the glow curve of the beta irradiated  $\text{SrAl}_2\text{O}_4:\text{Er}$ . At first sight the glow peak curve induced by beta irradiation resembles the glow curve of UV irradiated material, but in detail there are considerable changes in relative peak intensity, as well as displacements of the higher temperature peaks. There are also differences in the glow curves of Er and Eu doped samples. Nearly all the doped TL signals differ from those seen by beta irradiation of the undoped material. The implication is that the stability of charge in the trapping sites is influenced by the dopant and so, as expected, the TL is from closely related complex structures involving both trap and rare earth luminescence site. Figs. 12–14 exhibit different behaviours in many ways. Therefore it might be useful to show them in a table in order to emphasize the differences (Table 1).

There are two peaks at 125 and 545  $^\circ\text{C}$  in glow curve of the beta irradiated Eu doped  $\text{SrAl}_2\text{O}_4$  phosphor. Glow peak structure of the beta irradiated Eu doped  $\text{SrAl}_2\text{O}_4$  phosphor is somewhat

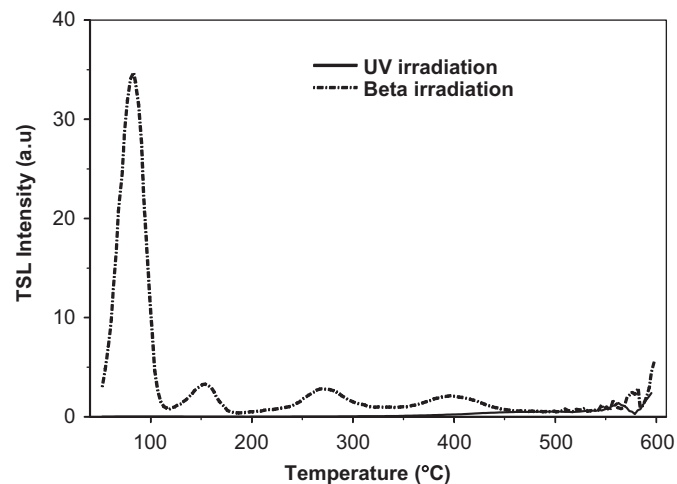


Fig. 12. TSL glow curves of undoped  $\text{SrAl}_2\text{O}_4$  irradiated with beta and UV radiation.

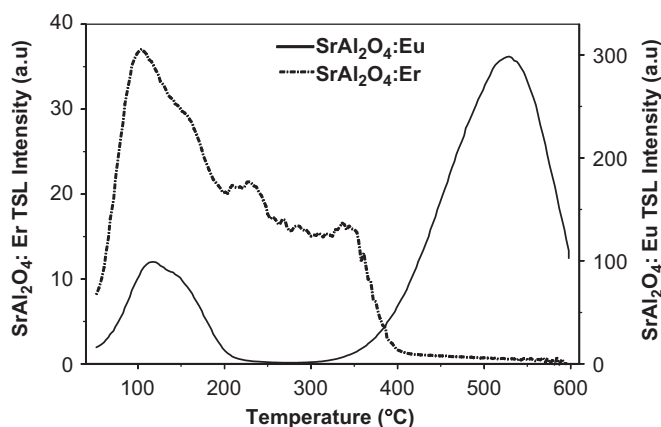


Fig. 13. TSL glow curves of Eu and Er doped  $\text{SrAl}_2\text{O}_4$  irradiated with UV radiation.

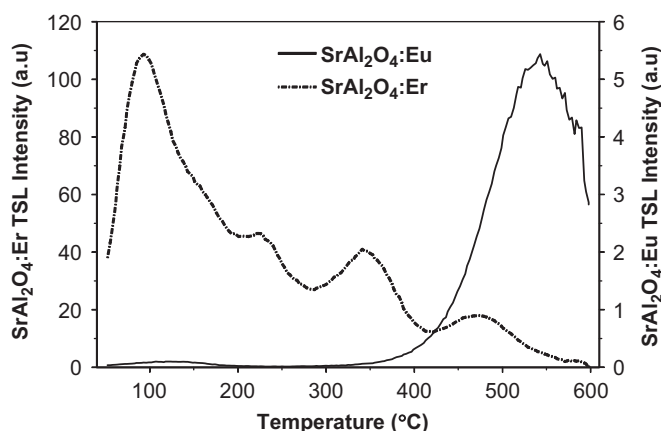


Fig. 14. TSL glow curves of Eu and Er doped  $\text{SrAl}_2\text{O}_4$  irradiated with beta radiation.

Table 1

Peak temperatures and intensity values of the  $\text{SrAl}_2\text{O}_4$ ,  $\text{SrAl}_2\text{O}_4:\text{Er}$  and  $\text{SrAl}_2\text{O}_4:\text{Eu}$ , respectively.

<b><math>\text{SrAl}_2\text{O}_4</math></b>				
<i>UV irradiation</i>				
Peak temp. ( $^\circ\text{C}$ )	–	–	–	–
Intensity	–	–	–	–
<i>Beta irradiation</i>				
Peak temp. ( $^\circ\text{C}$ )	82	153	270	397
Intensity	34.7	3.2	2.8	2.12
<b><math>\text{SrAl}_2\text{O}_4:\text{Er}</math></b>				
<i>UV irradiation</i>				
Peak temp. ( $^\circ\text{C}$ )	104	157	230	337
Intensity	37	29.5	21.4	16.5
<i>Beta irradiation</i>				
Peak temp. ( $^\circ\text{C}$ )	93	225	345	471
Intensity	108.7	46.4	40.3	17.9
<b><math>\text{SrAl}_2\text{O}_4:\text{Eu}</math></b>				
<i>UV irradiation</i>				
Peak temp. ( $^\circ\text{C}$ )	117	527	–	–
Intensity	99.1	298.5	–	–
<i>Beta irradiation</i>				
Peak temp. ( $^\circ\text{C}$ )	125	545	–	–
Intensity	0.1	5.4	–	–

similar to that of UV irradiated ones, but the maximum intensity of beta irradiated Eu doped sample is considerably lower compared to both undoped and also to Er doped  $\text{SrAl}_2\text{O}_4$  samples. Note however that the sensitivity of the TL system (filter and photomultiplier response) is far less favourable for detection of

the red Eu signal compared with the emission from Er. Furthermore, high and low temperature peak intensity of beta irradiated SrAl<sub>2</sub>O<sub>4</sub>:Eu is decreased by sixty and a thousand times compared to that of UV irradiated SrAl<sub>2</sub>O<sub>4</sub>:Eu, respectively. One must note that in visual applications of such phosphors the differences will be less as the response of the eye differs from that of the TL photomultiplier detection.

It is well known that in SrAl<sub>2</sub>O<sub>4</sub>:Eu phosphor, Eu<sup>2+</sup> ions are the luminescent centres, the luminescence is considered to be due to the transition from 5d level to 4f level of Eu<sup>2+</sup>. Upon the exposure to the ultraviolet lights, electrons of Eu<sup>2+</sup> ion in the 4f level transfer to 5d level, and holes are produced. Some of free holes released thermally to the valence band. When the excitation source was removed, the excited Eu<sup>+</sup> is able to relax to the stable state (Eu<sup>+</sup>)\*. The trapped holes are released thermally to the valence band and migrate to recombine with the excess electron in the metastable state (Eu<sup>+</sup>)\* site and lead to the long afterglow. The long phosphorescence depends on the depth and the density of the hole trap.

#### 4. Conclusions

In this work, the SrAl<sub>2</sub>O<sub>4</sub> compound doped with different rare earth ions has been investigated by XRD, Raman spectroscopy, PL and TSL. The formation of monoclinic polymorphs has been confirmed by XRD and Raman spectroscopy. The SEM investigations suggest the formation of crystalline particles with large sizes.

This spectroscopic study has revealed fundamental information regarding the luminescence features of Er<sup>3+</sup> ions in SrAl<sub>2</sub>O<sub>4</sub> phosphors. In particular, the estimated peak value of emission cross section for the potential <sup>4</sup>I<sub>13/2</sub>–<sup>4</sup>I<sub>15/2</sub> laser transition around 1544 nm is advantageously high and the dynamics of energy transfer from pump bands to the upper laser level <sup>4</sup>I<sub>13/2</sub> is favourable for laser operation.

The excitation and emission spectra indicate the Eu<sup>3+</sup> and Eu<sup>2+</sup> ions coexist in the sample. This suggests that some kinds of defects are required inside the network in order to favour the electron–hole recombination. Excitation contains broad excitation band centred at 370 nm and is anticipated to be that of some ITS located between the band gap. Characteristic emission for Eu is obtained with maxima at 620 nm followed by shoulder at 650 nm. In the present case, typical f–f transitions of rare earth ions are observed.

Pure host material (SrAl<sub>2</sub>O<sub>4</sub>) does not exhibits any TSL response following excitation UV, but an attempt was done to produce more efficient materials which are sensitive to UV excitation. There is a clear influence on the TSL response from the host material which contains Eu and Er dopants. In both cases it was observed that the doping of Eu and Er to the host material

have led to the formation of UV-sensitivity. TSL characterizations observed following beta irradiation of pure and Er doped SrAl<sub>2</sub>O<sub>4</sub> are similar to each other. It was observed that when the results are compared to those obtained with UV and beta irradiation some of the similarities may result from the same luminescence centres which are responsible for the TSL. It is also clear that TSL intensity of Er doped host material after beta irradiation is much higher than UV irradiation (i.e. by factors of up to 3.5) Both types of treatments (UV and beta) indicate that TSL could be used as a non-destructive monitor of material quality and reproducibility of preparation procedure. It is not yet possible to offer detailed models of the TSL response but further investigations are in progress to elucidate the influence of other rare-earth ions on SrAl<sub>2</sub>O<sub>4</sub>.

#### Acknowledgements

The work described here was financially supported by Scientific Research Coordinate Unit of Celal Bayar University project FEF 2009-06347 which was accepted as a Ph.D. project of one of the authors (M.Ayvacili) under the supervision of Prof. Dr. N. Can. We are grateful to Dr. M. Hatipolu for the analyses in the Raman spectroscopy of Dokuz Eyll University (Turkey). Er PL spectrum and PL lifetime measurements were carried out at Boston University in Prof. L. Dal Negro's laboratory.

#### References

- [1] T. Katsumata, K. Sasajima, T. Nabae, S. Komuro, T. Morikawa, J. Am. Ceram. Soc. 81 (2) (1998) 413.
- [2] T. Matsuzawa, Y. Aoki, N. Takeuchi, Y. Murayama, J. Electrochem. Soc. 143 (8) (1996) 2670.
- [3] S.K. Sharma, Shreyas S. Pitale, M. Manzar Malik, M.S. Qureshi, R.N. Dubey, J. Alloy Compd 482 (2009) 468.
- [4] F. Clabau, X. Rocquefelte, S. Jobic, P. Deniard, M.-H. Whangbo, A. Garcia, T. Le Mercier, Chem. Mater. 17–15 (2005) 3904.
- [5] Y. Lin, Z. Tang, Z. Zhang, Mater. Lett. 51 (1) (2001) 14–18.
- [6] C. Chang, D. Mao, J. Shen, C. Feng, J. Alloy Compd 348 (2003) 224.
- [7] R. Zhong, J. Zhang, X. Zhang, S. Lu, X. Wang, J. Lumin. 119–120 (2006) 327.
- [8] P.J.R. Montes, M.E.G. Valerio, J. Lumin. 130 (2010) 1525.
- [9] K. Fukuda, K. Fukushima, J. Solid State Chem. 178 (2005) 2709.
- [10] S.H.M. Poort, W.P. Blokpoel, G. Blasse, Chem. Mater. 7 (1995) 1547.
- [11] E. Cordocillo, B. Julian-Lopez, M. Martinez, M.L. Sanjun, P. Escribano, J. Alloy. Compd. 484 (2009) 693.
- [12] X. Yu, C. Zhou, X. He, Z. Peng, S. Yang, Mater. Lett. 58 (2004) 1087.
- [13] P. Dorenbos, J. Lumin. 104 (2003) 239.
- [14] P. Dorenbos, J. Electrochem. Soc. 152 (7) (2005) H107.
- [15] L.C. Courrol, L.R.P. Kassab, M.E. Fukumoto, N.U. Wetter, S.H. Tatumi, N.I. Morimoto, J. Lumin. 102–103 (2003) 91.
- [16] P. Page, R. Ghildiyal, K.V.R. Murthy, Mater. Res. Bull. 41 (2006) 1854.
- [17] Y. Pan, H.H.-Y. Sung, H. Wu, J. Wang, X. Yang, M. Wu, Q. Su, Mater. Res. Bull. 41 (2006) 225.
- [18] H. Ryu, K.S. Bartwal, Physica B 404 (2009) 1714.
- [19] P.J.R. Montes, M.E.G. Valerio, G.M. Azevedo, Nucl. Instrum. Meth. B 266 (2008) 2923.